Figure S1

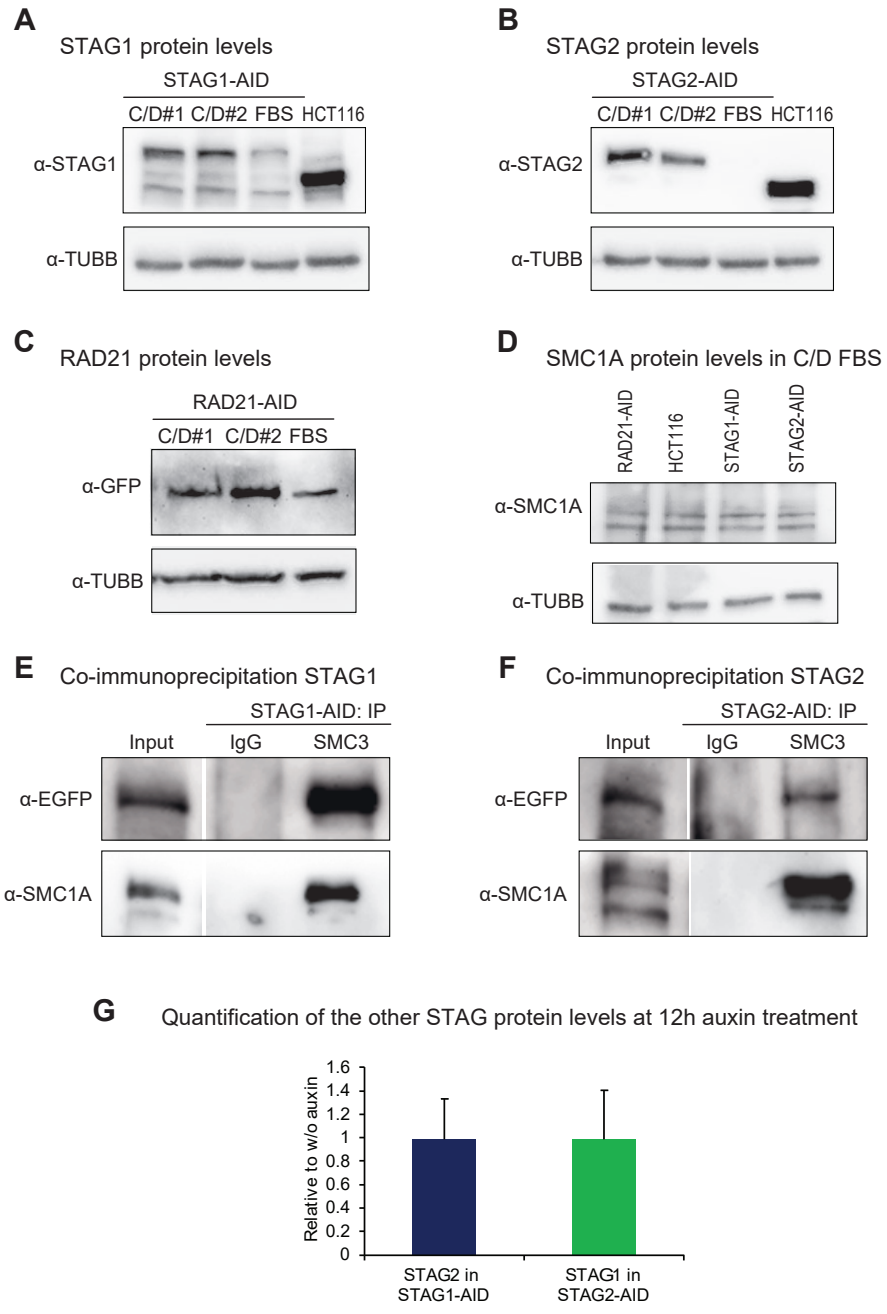
A
STAG1 protein levels
STAG1-AID
C/D#1 C/D#2 FBS HCT116
α-STAG1
α-TUBB
B
STAG2 protein levels
STAG2-AID
C/D#1 C/D#2 FBS HCT116
α-STAG2
α-TUBB
C
RAD21 protein levels
RAD21-AID
C/D#1 C/D#2 FBS
α-GFP
α-TUBB
D
SMC1A protein levels in C/D FBS
RAD21-AID
HCT116
STAG1-AID
STAG2-AID
α-SMC1A
α-TUBB
E
Co-immunoprecipitation STAG1
STAG1-AID: IP
Input
IgG
SMC3
α-EGFP
α-SMC1A
F
Co-immunoprecipitation STAG2
STAG2-AID: IP
Input
IgG
SMC3
α-EGFP
α-SMC1A
G
Quantification of the other STAG protein levels at 12h auxin treatment
Relative to w/o auxin
1.6
1.4
1.2
1
0.8
0.6
0.4
0.2
0
STAG2 in STAG1-AID
STAG1 in STAG2-AID

Supplementary figures:

Figure S1 Stability of AID-tagged proteins in different culture media and integration of the AID-tagged subunits in the cohesin core complex

A-C) Degradation by the AID-tag can be induced by components of the culture medium, as also described (Natsume et al. 2013) (Yesbolatova et al. 2019), leading to strongly reduced levels of the AID-tagged protein compared to wildtype levels. We tested McCoy medium supplemented with a standard fetal bovine serum batch (FBS) and two batches of commercially available charcoal/dextran treated FBS (C/D) and noted that the treated FBS batches retain the levels of AID-tagged proteins in case of STAG1-AID (A), STAG2-AID (B) and also RAD21-AID (C) much better than standard FBS. The effect on STAG1-AID and STAG2-AID is stronger than on RAD21-AID, likely since these subunits are not essential for cell viability (van der Lelij et al. 2017). **D)** Levels of SMC1A in RAD21-AID, STAG1-AID and STAG2-AID cells compared to wildtype levels. **E, F)** Immunoprecipitation of SMC3 from STAG1-AID (E) and STAG2-AID (F) cells demonstrates that the modified subunits are incorporated in the cohesin complex. **G)** Quantitation of the respective other STAG protein level after auxin-mediated degradation of STAG1 or STAG2. STAG2 levels were quantified in STAG1-AID cells and STAG1 levels in STAG2-AID cells after 12 hours auxin treatment and normalized to no auxin treatment. Three independent western blots corresponding to the ones shown in Figures 1 C and D were quantified using Image J.

Figure S2

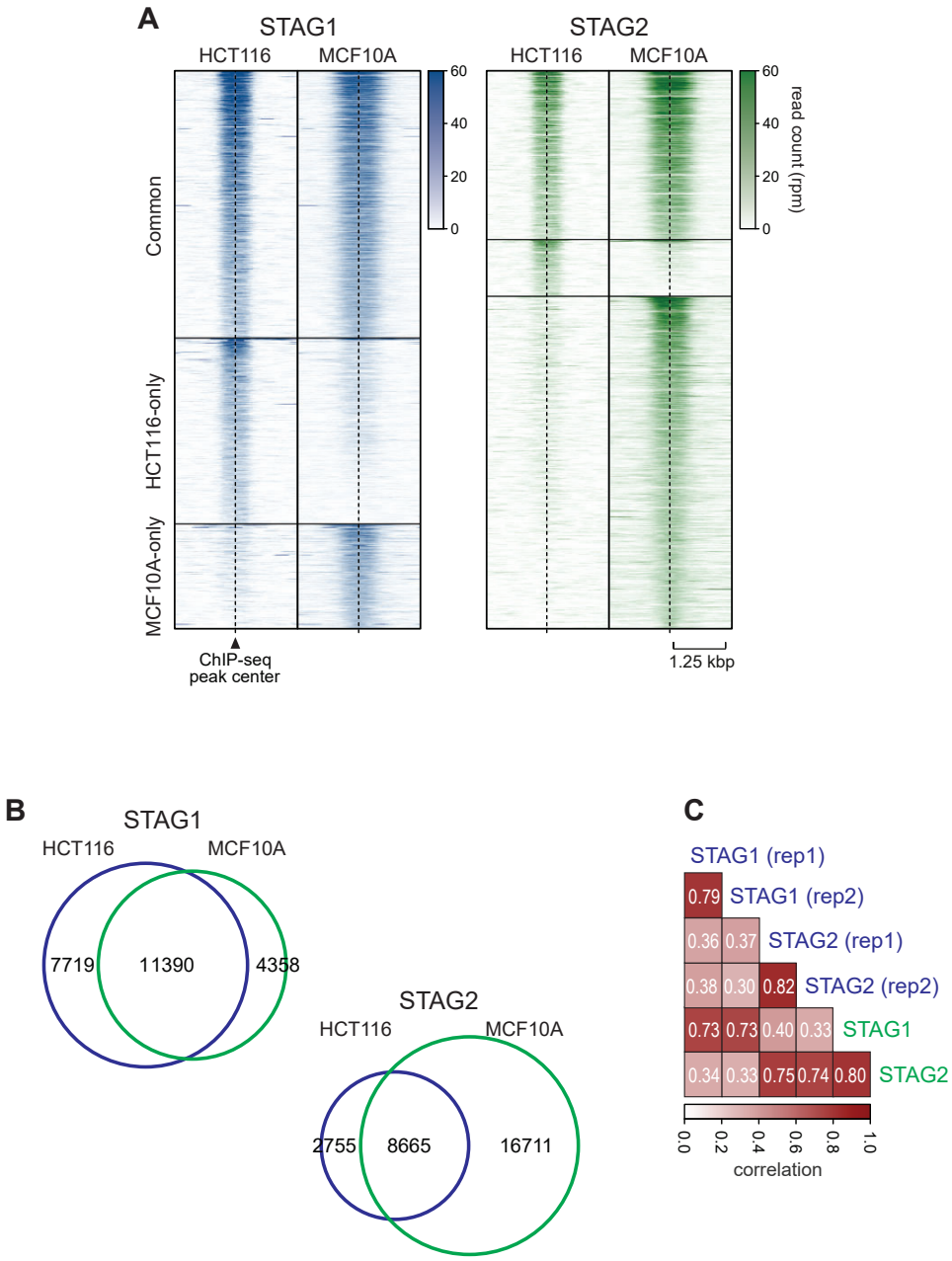
A
STAG1
HCT116
MCF10A
STAG2
HCT116
MCF10A
60
40
20
0
read count (rpm)
Common
HCT116-only
MCF10A-only
ChIP-seq
peak center
1.25 kbp
B
STAG1
HCT116
MCF10A
7719
11390
4358
STAG2
HCT116
MCF10A
2755
8665
16711
C
STAG1 (rep1)
0.79
STAG1 (rep2)
0.36
0.37
STAG2 (rep1)
0.38
0.30
0.82
STAG2 (rep2)
0.73
0.73
0.40
0.33
STAG1
0.34
0.33
0.75
0.74
0.80
STAG2
0.0
0.2
0.4
0.6
0.8
1.0
correlation

Figure S2 Comparison of ChIP-sequencing data from HCT116 (this manuscript) with MCF10A cells (Koijc et al., 2018)

A) Heatmaps showing the ChIP-sequencing signals of STAG1 (blue) and STAG2 (green) from STAG1-AID and STAG2-AID HCT116 cells (this manuscript, using anti-EGFP antibodies) and MCF10A cells (Kojic et al. 2018). Common and unique sites from both cell types are shown. **B)** Number of shared or unique peaks for STAG1 and STAG2 in STAG1-AID or STAG2-AID cells and MCF10A cells (Kojic et al. 2018). **C)** Correlation between the different samples and replicates of the ChIP-seq experiments in this study and in Koijc et al., 2018 (Kojic et al. 2018).

Figure S3

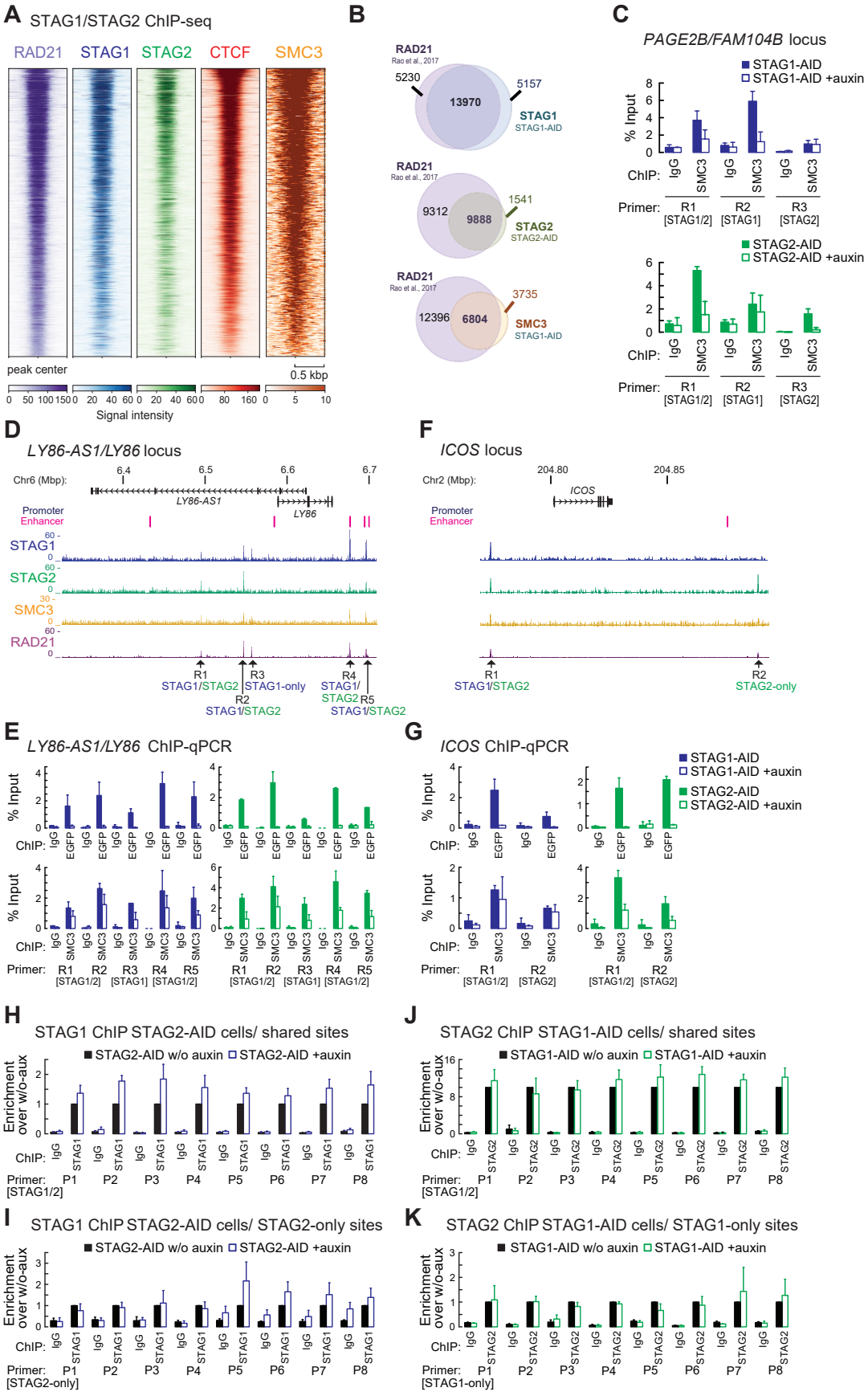
A
STAG1/STAG2 ChIP-seq
RAD21
STAG1
STAG2
CTCF
SMC3
peak center
0.5 kbp
Signal intensity
B
RAD21
Rao et al., 2017
5230
13970
5157
STAG1
STAG1-AID
9312
9888
1541
STAG2
STAG2-AID
12396
6804
3735
SMC3
C
PAGE2B/FAM104B locus
STAG1-AID
STAG1-AID +auxin
% Input
ChIP:
Primer:
R1 [STAG1/2]
R2 [STAG1]
R3 [STAG2]
STAG2-AID
STAG2-AID +auxin
D
LY86-AS1/LY86 locus
Chr6 (Mbp):
LY86-AS1
LY86
Promoter
Enhancer
STAG1
STAG2
SMC3
RAD21
R1 STAG1/STAG2
R2 STAG1/STAG2
R3 STAG1-only
R4 STAG1/STAG2
R5 STAG1/STAG2
F
ICOS locus
Chr2 (Mbp):
ICOS
R1 STAG1/STAG2
R2 STAG2-only
E
LY86-AS1/LY86 ChIP-qPCR
% Input
ChIP:
Primer:
R1 [STAG1/2]
R2 [STAG1]
R3 [STAG1]
R4 [STAG1/2]
R5 [STAG1/2]
G
ICOS ChIP-qPCR
STAG1-AID
STAG1-AID +auxin
STAG2-AID
STAG2-AID +auxin
R1 [STAG1/2]
R2 [STAG2]
H
STAG1 ChIP STAG2-AID cells/ shared sites
STAG2-AID w/o auxin
STAG2-AID +auxin
Enrichment over w/o-aux
Primer: [STAG1/2]
J
STAG2 ChIP STAG1-AID cells/ shared sites
STAG1-AID w/o auxin
STAG1-AID +auxin
I
STAG1 ChIP STAG2-AID cells/ STAG2-only sites
Primer: [STAG2-only]
K
STAG2 ChIP STAG1-AID cells/ STAG1-only sites
Primer: [STAG1-only]

Figure S3 STAG1 and STAG2 have overlapping as well as discrete binding sites

A) Heatmaps showing the ChIP-seq signals for RAD21, STAG1, STAG2, CTCF and SMC3. RAD21 and CTCF ChIP-seq data are from Rao et al., 2017 (Rao et al. 2017). **B)** Venn diagrams showing the number of shared peaks between RAD21 ChIP-seq data from Rao et al., 2017 and STAG1, STAG2 and SMC3 ChIP-seq data presented in this manuscript. **C)** ChIP-qPCR showing that SMC3-binding at sites in the *PAGE2B/FAM104B* locus (also in Figure 2D, E) is reduced upon degradation of STAG1 or STAG2 on STAG1- or STAG2-only sites but is also on STAG1/STAG2-shared sites. **D, F)** Two more loci were analyzed to confirm the presence of STAG1 and STAG2-only sites, the *LY86-AS1/LY86* locus (D) and the *ICOS* locus (F). **E, G)** STAG1-only, STAG2-only and STAG1/2 shared sites at the *LY86-AS1/LY86* locus (E) and the *ICOS* locus (G) were tested in anti-EGFP ChIP (upper panel) and SMC3 ChIP from STAG1-AID and STAG2-AID cells w/o and with auxin treatment. **H, I)** STAG1 ChIP was performed from STAG2-AID cells with and without auxin treatment to test whether STAG1 accumulates more at these sites after STAG2 depletion. STAG1/STAG2 shared sites (H) and STAG2-only sites (I) were analyzed. **J, K)** STAG2 ChIP was performed from STAG1-AID cells with and without auxin treatment to test whether more STAG2 accumulates more at these sites after STAG1 depletion. STAG1/STAG2 shared sites (J) and STAG1-only (K) sites were analyzed.

Figure S4

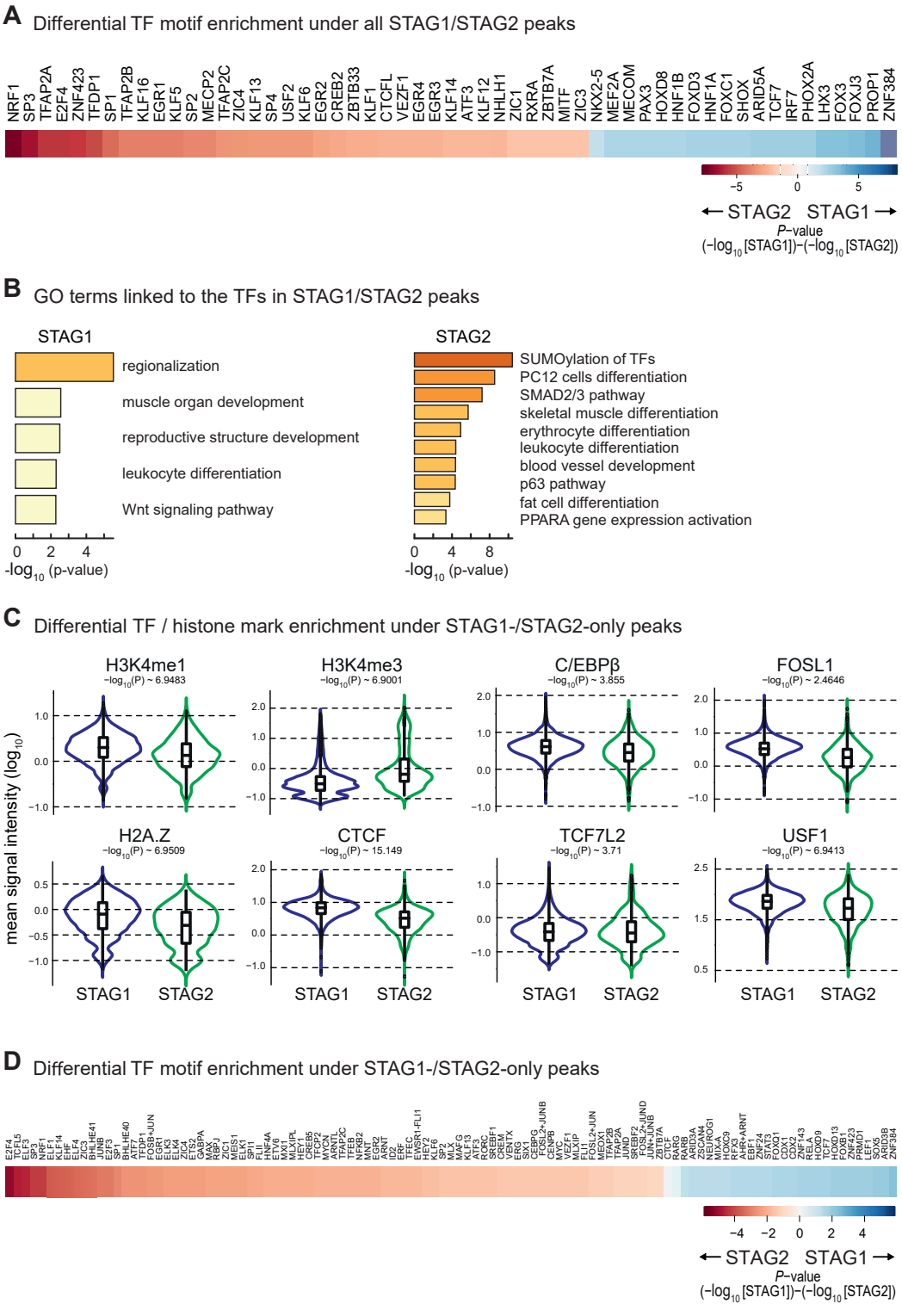
A
Differential TF motif enrichment under all STAG1/STAG2 peaks
NRF1 SP3 TFAP2A E2F4 ZNF423 TFDP1 SP1 TFAP2B KLF16 EGR1 KLF5 SP2 MECP2 TFAP2C ZIC4 KLF13 SP4 USF2 KLF6 EGR2 CREB2 ZBTB33 KLF1 CTCFL VEZF1 EGR4 EGR3 KLF14 ATF3 KLF12 NHLH1 ZIC1 RXRA ZBTB7A MITF ZIC3 NKX2-5 MEF2A MECOM PAX3 HOXD8 HNF1B FOXD3 HNF1A FOXC1 SHOX ARID5A TCF7 IRF7 PHOX2A LHX3 FOX3 FOXJ3 PROP1 ZNF384
−5 0 5
← STAG2 STAG1 →
P–value
(−log10[STAG1])−(−log10[STAG2])
B
GO terms linked to the TFs in STAG1/STAG2 peaks
STAG1
regionalization
muscle organ development
reproductive structure development
leukocyte differentiation
Wnt signaling pathway
0 2 4
-log10 (p-value)
STAG2
SUMOylation of TFs
PC12 cells differentiation
SMAD2/3 pathway
skeletal muscle differentiation
erythrocyte differentiation
leukocyte differentiation
blood vessel development
p63 pathway
fat cell differentiation
PPARA gene expression activation
0 4 8
-log10 (p-value)
C
Differential TF / histone mark enrichment under STAG1-/STAG2-only peaks
H3K4me1
−log10(P) ~ 6.9483
H3K4me3
−log10(P) ~ 6.9001
C/EBPβ
−log10(P) ~ 3.855
FOSL1
−log10(P) ~ 2.4646
H2A.Z
−log10(P) ~ 6.9509
CTCF
−log10(P) ~ 15.149
TCF7L2
−log10(P) ~ 3.71
USF1
−log10(P) ~ 6.9413
mean signal intensity (log10)
STAG1 STAG2
D
Differential TF motif enrichment under STAG1-/STAG2-only peaks
−4 −2 0 2 4
← STAG2 STAG1 →
P–value
(−log10[STAG1])−(−log10[STAG2])

Figure S4 Enrichment of transcription factor (TF) motifs and signals at STAG1 and STAG2 sites

A) The probability of the presence of another TF at the STAG1/STAG2-shared binding sites was calculated based on the accessibility of the sites (DNase hypersensitivity) and the presence of TF motifs (Lin et al. 2015). The differences of enrichment between STAG1 and STAG2 are plotted as heatmap. **B)** GO-term analysis of the TFs plotted in (A) using Metascape (Zhou et al. 2019). **C)** Enrichment of histone marks and TFs at STAG1- and STAG2-only peaks. Published datasets for HCT116 cells were used (Rao et al. 2017; Davis et al. 2018) (Table S8). Wilcoxon-Mann-Whitney U test with Benjamini-Hochberg correction p-values are shown. **D)** The probability of the presence of another TF at the STAG1- and STAG2-only binding sites was calculated based on the accessibility of the sites (DNase hypersensitivity) and the presence of transcription factor motifs (Lin et al. 2015). The differences of enrichment between STAG1 and STAG2 are plotted as heatmap.

Figure S5

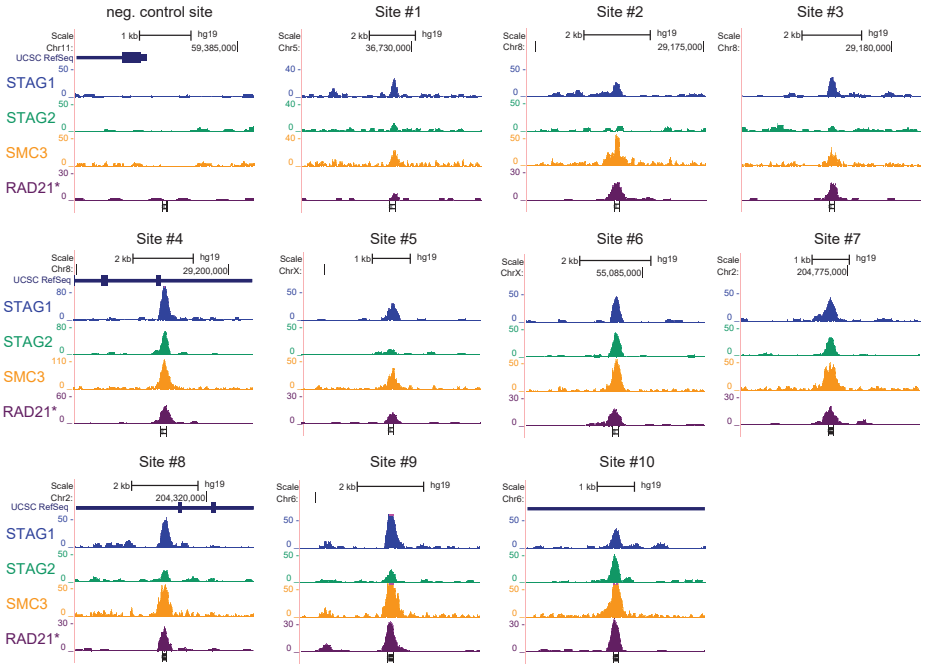
neg. control site
Site #1
Site #2
Site #3
Site #4
Site #5
Site #6
Site #7
Site #8
Site #9
Site #10
STAG1
STAG2
SMC3
RAD21*
UCSC RefSeq
hg19

Figure S5 STAG1/STAG2 sites investigated by Re-CHIP

ChIP-sequencing profiles for STAG1, STAG2, SMC3 and RAD21 (Rao et al. 2017) of the ten positive sites and one negative site investigated by Re-ChIP and qPCR. The positions of the qPCR primers are indicated below the ChIP-seq tracks.

Figure S6

Immunostaining of human skin fibroblasts and dSTORM experiments with secondary antibodies only

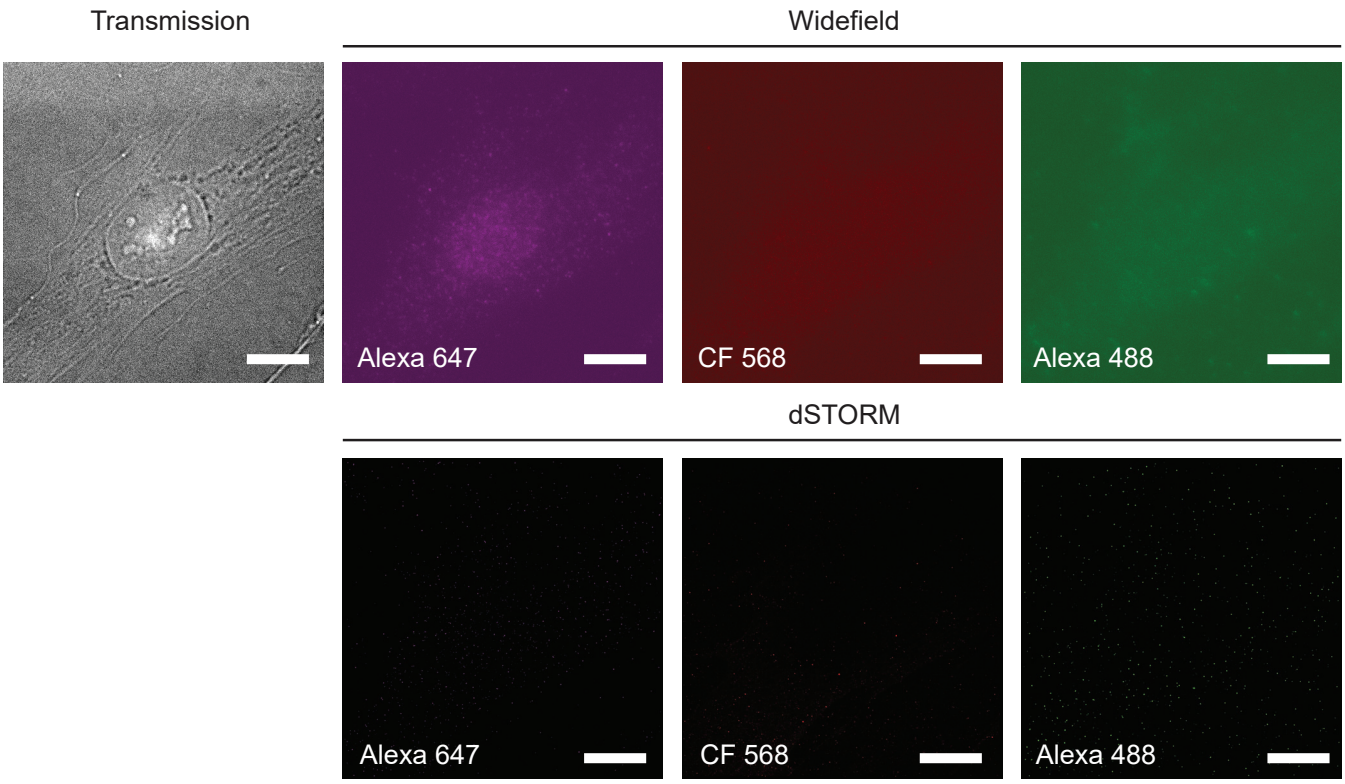

Scale bar = 5 µm

Figure S6 Immunostaining and dSTORM of fibroblasts using secondary antibodies only

Human skin fibroblasts were treated with the identical protocol for immunostaining as described for the dSTORM sample preparation in the Supplemental Methods section, except that the primary antibody was omitted. The secondary antibodies used were donkey-anti-rabbit Alexa647 (Jackson Immuno Research 711-605-152), donkey-anti-goat Alexa488 (Thermo Fisher Scientific A11055), donkey-anti-mouse CF568 (Biotium #20105-1). The upper panel shows a transmission light microscopy image to indicate the position of the cell nucleus and widefield images (contrast enhanced to show low residual signal) of the three different colors. The lower panel shows the accumulated dSTORM signal from 12000 frames. These signals were too sparse to perform clustering. Additionally, detected molecules were randomly distributed over the complete imaged area and the nucleus was not discernable in the reconstructed STORM images. This in contrast to the samples stained also with specific primary antibodies.

Figure S7

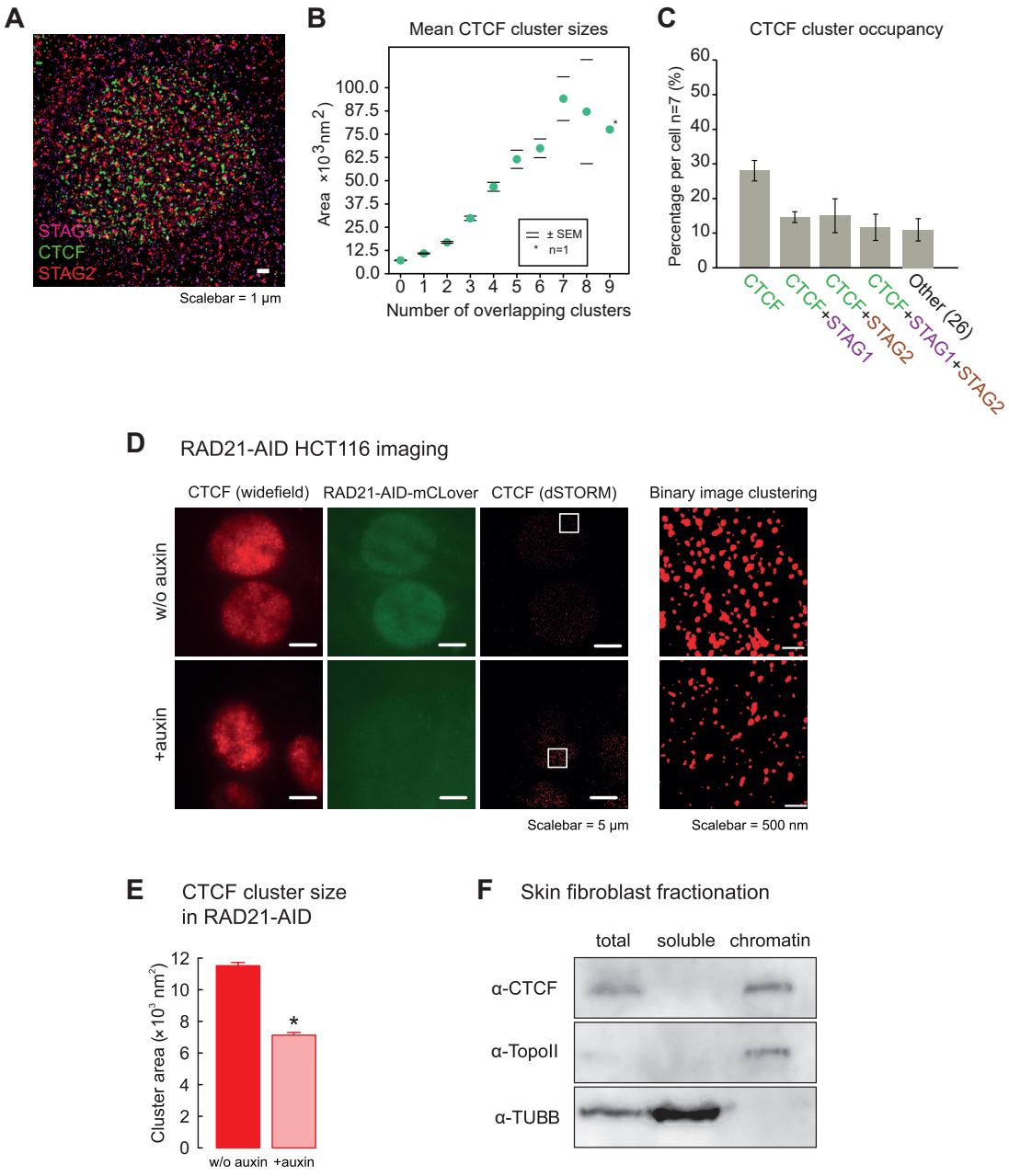
A
STAG1
CTCF
STAG2
Scalebar = 1 µm
B
Mean CTCF cluster sizes
Area ×10^3nm^2)
100.0
87.5
75.0
62.5
50.0
37.5
25.0
12.5
0.0
0 1 2 3 4 5 6 7 8 9
Number of overlapping clusters
± SEM
n=1
C
CTCF cluster occupancy
Percentage per cell n=7 (%)
60
50
40
30
20
10
0
CTCF
CTCF+STAG1
CTCF+STAG2
CTCF+STAG1+STAG2
Other (26)
D
RAD21-AID HCT116 imaging
CTCF (widefield)
RAD21-AID-mCLover
CTCF (dSTORM)
Binary image clustering
w/o auxin
+auxin
Scalebar = 5 µm
Scalebar = 500 nm
E
CTCF cluster size
in RAD21-AID
Cluster area (×10^3 nm^2)
12
10
8
6
4
2
0
*
w/o auxin
+auxin
F
Skin fibroblast fractionation
total
soluble
chromatin
α-CTCF
α-TopoII
α-TUBB

Figure S7 Single molecule localization

A) Merged reconstructed triple color dSTORM image of a single nucleus stained for STAG1 (magenta), STAG2 (red) and CTCF (green). The images were analyzed with the same pipeline as shown in Fig. 3D. **B)** The cluster area size (nm^2) for CTCF is plotted grouped per number of adherent clusters of STAG1 or STAG2. **C)** Frequency of CTCF cluster groups per cell measured for 7 cells. All CTCF clusters falling in other groups are depicted as "Others". This group contains 26 subgroups, eg. adhering to more than 2 clusters or 2 clusters of the same STAG. All error bars show standard error of the mean (+/- SEM). **D)** dSTORM using anti-CTCF was performed in HCT116 RAD21-AID cells (Natsume et al. 2016) w/o and with auxin treatment for 6 hours and the size of the CTCF signal clusters analyzed as in Figure 3D. **E)** The size of the CTCF clusters decreases after RAD21 degradation (+/- standard deviation of mean - SEM; *t*-test p-value is indicated, * P< 0.05). **F)** Fractionation of human skin fibroblasts used for dSTORM in Figure 3 in soluble fraction and chromatin-bound fraction. Western blotting with anti-CTCF shows that CTCF is not detectable in the soluble fraction and therefore fully chromatin-bound. As controls for the chromatin-bound fraction anti-Topoisomerase II was used and anti-tubulin as control for the soluble fraction.

Figure S8

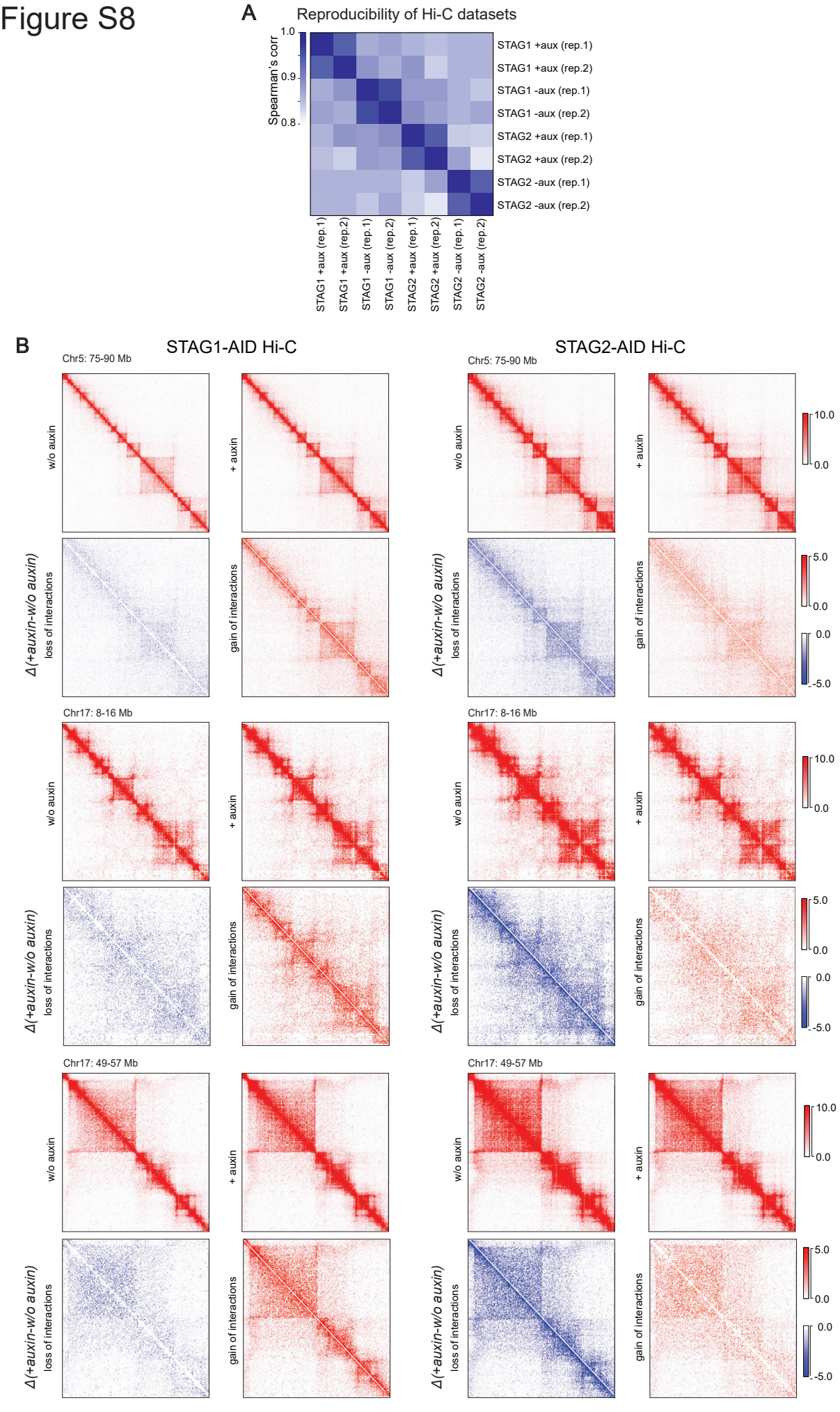
A
Reproducibility of Hi-C datasets
Spearman's corr
1.0
0.9
0.8
STAG1 +aux (rep.1)
STAG1 +aux (rep.2)
STAG1 -aux (rep.1)
STAG1 -aux (rep.2)
STAG2 +aux (rep.1)
STAG2 +aux (rep.2)
STAG2 -aux (rep.1)
STAG2 -aux (rep.2)
B
STAG1-AID Hi-C
STAG2-AID Hi-C
Chr5: 75-90 Mb
Chr17: 8-16 Mb
Chr17: 49-57 Mb
w/o auxin
+ auxin
Δ(+auxin-w/o auxin)
loss of interactions
gain of interactions
10.0
0.0
5.0
0.0
0.0
-5.0

Figure S8 STAG1 and STAG2 affect long-range interactions differently

A) Correlation between the different samples and replicates of the Hi-C experiments in this study.

B) Zoom-in into the contact maps for STAG1-AID cells (left) and STAG2-AID cells (right) for regions on Chromosome 5 and Chromosome 17. The maps for untreated cells (w/o auxin), treated cells (+auxin) and the differential interaction maps split in loss of interactions (blue) and gain of interactions (red) are shown.

Figure S9

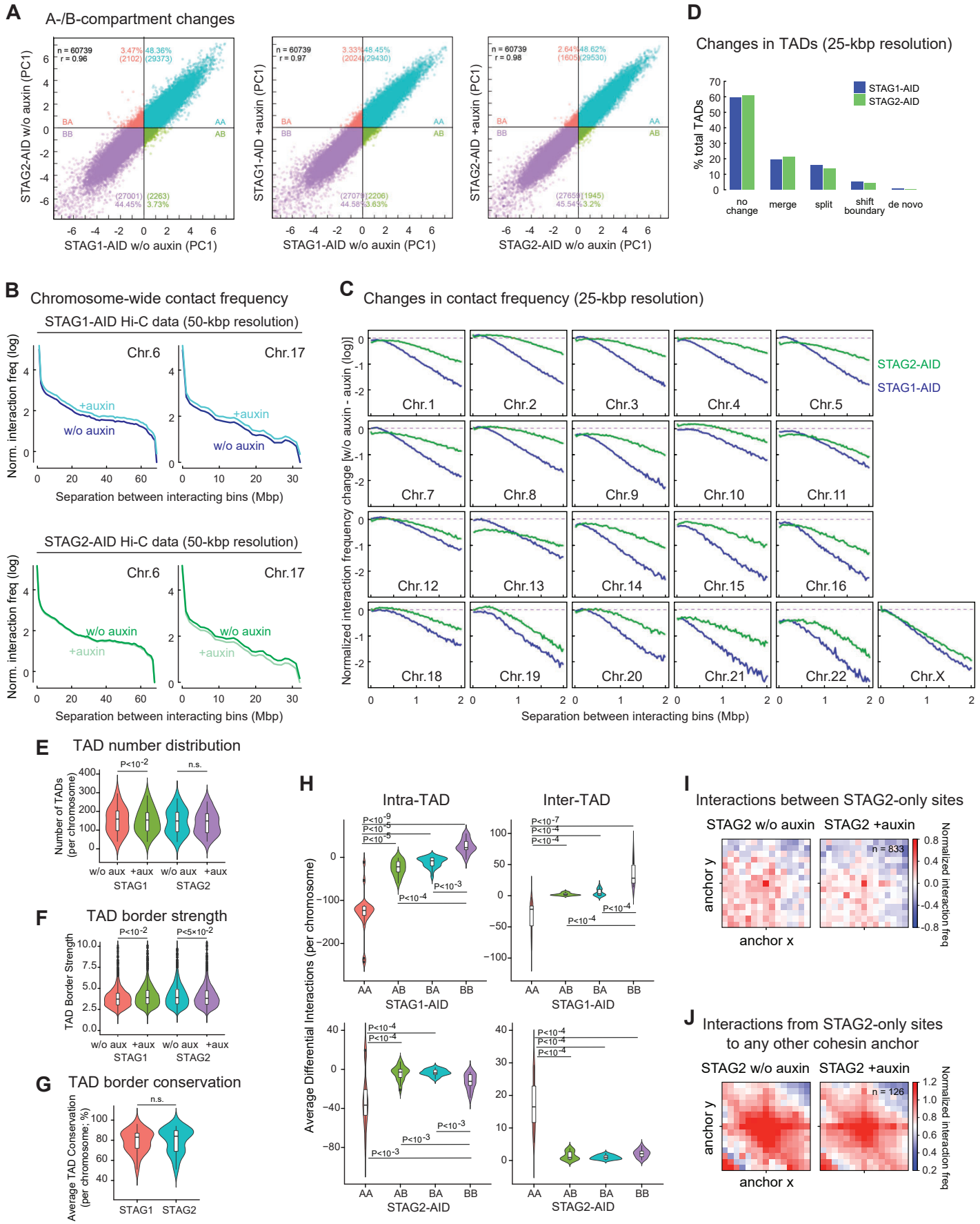
A
A-/B-compartment changes
STAG2-AID w/o auxin (PC1)
STAG1-AID w/o auxin (PC1)
STAG1-AID +auxin (PC1)
STAG2-AID +auxin (PC1)
BA
BB
AA
AB
D
Changes in TADs (25-kbp resolution)
% total TADs
STAG1-AID
STAG2-AID
no change
merge
split
shift boundary
de novo
B
Chromosome-wide contact frequency
STAG1-AID Hi-C data (50-kbp resolution)
STAG2-AID Hi-C data (50-kbp resolution)
Norm. interaction freq (log)
Chr.6
Chr.17
+auxin
w/o auxin
Separation between interacting bins (Mbp)
C
Changes in contact frequency (25-kbp resolution)
Normalized interaction frequency change [w/o auxin - auxin (log)]
Chr.1
Chr.2
Chr.3
Chr.4
Chr.5
Chr.7
Chr.8
Chr.9
Chr.10
Chr.11
Chr.12
Chr.13
Chr.14
Chr.15
Chr.16
Chr.18
Chr.19
Chr.20
Chr.21
Chr.22
Chr.X
E
TAD number distribution
Number of TADs (per chromosome)
w/o aux
+aux
STAG1
STAG2
F
TAD border strength
TAD Border Strength
G
TAD border conservation
Average TAD Conservation (per chromosome; %)
H
Intra-TAD
Inter-TAD
Average Differential Interactions (per chromosome)
I
Interactions between STAG2-only sites
STAG2 w/o auxin
STAG2 +auxin
anchor y
anchor x
Normalized Interaction freq
J
Interactions from STAG2-only sites to any other cohesin anchor

Figure S9 STAG1 and STAG2 affects long-range interactions differently

A) Contacts between and within A and B compartments are correlated between the contact matrices of STAG1-AID and STAG2-AID cells without (w/o) auxin and then with and without auxin in STAG1-AID and STAG2-AID cells. Total contacts observed, correlation coefficient as well as the percentage and number of the contacts between the specific compartments are indicated. PC1 = principal component 1. **B)** Normalized interaction frequencies are plotted against the distance between interacting bins (at 50 kb resolution) without and with auxin-mediated degradation for STAG1-AID and STAG2-AID cells. Chromosomes 6 and 17 are shown. **C)** Change of contacts between bins (at 25 kb resolution) relative to the separation of the contacting fragments after STAG1 or STAG2 degradation are shown for all chromosomes, except Chromosomes 6 and 17 that are displayed in Fig. 4E. **D)** Comparison of TADs before and after degradation of STAG1 or STAG2. **E)** Changes in STAG1-AID and STAG2-AID cells before and after auxin treatment in terms of number of TADs per chromosome. **F)** Changes in STAG1-AID and STAG2-AID cells before and after auxin treatment in terms of TAD border strength. **G)** Changes in STAG1-AID and STAG2-AID cells before and after auxin treatment in terms of TAD border conservation. **H)** Intra-TAD or inter-TAD changes of contacts after STAG1 or STAG2 degradation between and within A and B compartments. Statistical test performed in E-H: Wilcoxon-Mann-Whitney U test; p-values corrected by the Benjamini-Hochberg method are indicated. **I)** Aggregate peak analysis of STAG2-only peaks showing that STAG2-only peaks do not contact each other. **J)** Aggregate peak analysis of the contacts of STAG2-only peaks to other cohesin sites showing that these contacts persist after STAG2 degradation.

Figure S10

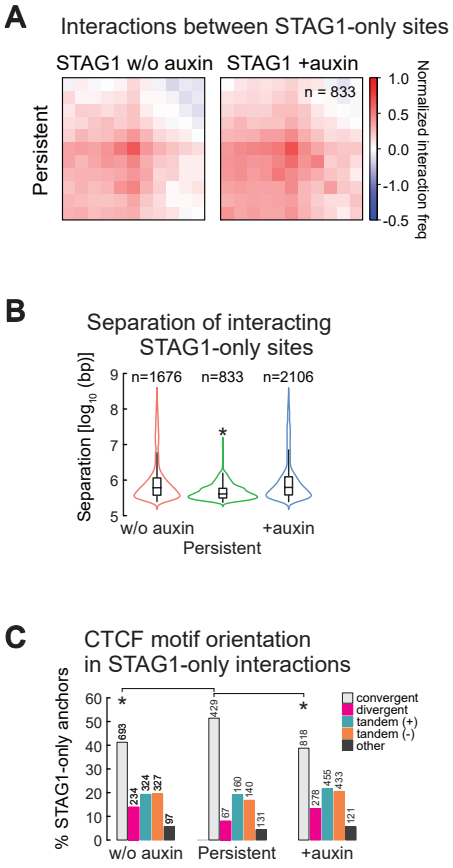
A
Interactions between STAG1-only sites
STAG1 w/o auxin
STAG1 +auxin
n = 833
Persistent
1.0
0.5
0.0
-1.0
-0.5
Normalized interaction freq
B
Separation of interacting
STAG1-only sites
Separation [log10 (bp)]
n=1676
n=833
n=2106
9
8
7
6
5
w/o auxin
+auxin
Persistent
C
CTCF motif orientation
in STAG1-only interactions
% STAG1-only anchors
60
50
40
30
20
10
0
683
234
324
327
97
429
67
160
140
131
818
278
455
433
121
w/o auxin
Persistent
+auxin
convergent
divergent
tandem (+)
tandem (-)
other

Figure S10 Contacts between STAG1-only sites

A) Aggregate peak analysis of persistent contacts between STAG1-only sites without (w/o) and with auxin in STAG1-AID cells. **B)** Number and distances between interacting bins with STAG1-only sites with contacts in STAG1-AID cells without (w/o) auxin, with auxin (+auxin) and persistent in both situations. **C)** Orientation of the CTCF motif at STAG1-only sites engaged in the different contact categories shown in (B) without (w/o) auxin, with auxin and persistent. Wilcoxon-Mann-Whitney U test p-values with Benjamini-Hochberg correction are shown, * $P < 0.05$.

Figure S11

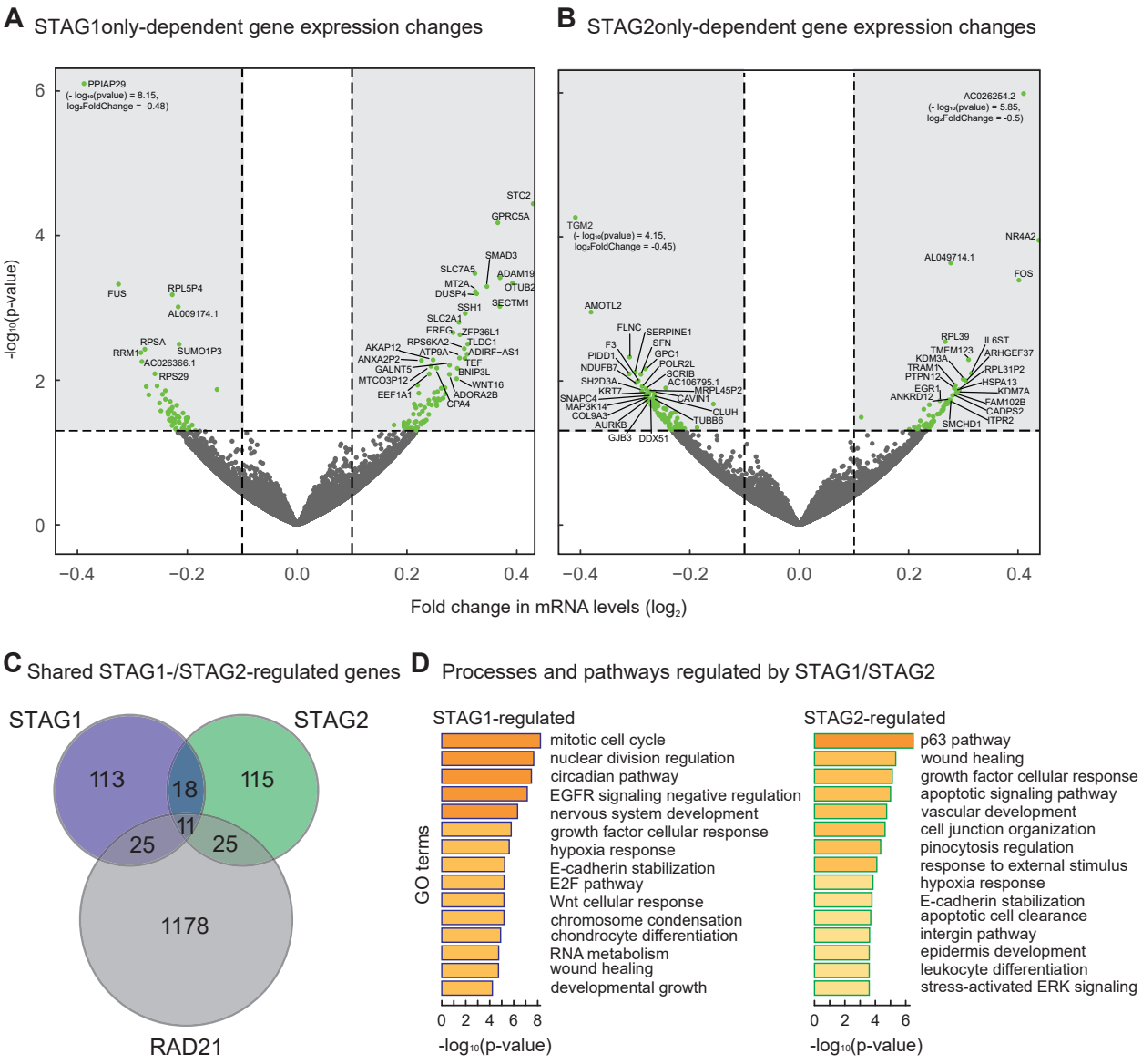
A STAG1only-dependent gene expression changes
B STAG2only-dependent gene expression changes
PPIAP29
(- log10(pvalue) = 8.15,
log2FoldChange = -0.48)
AC026254.2
(- log10(pvalue) = 5.85,
log2FoldChange = -0.5)
TGM2
(- log10(pvalue) = 4.15,
log2FoldChange = -0.45)
-log10(p-value)
Fold change in mRNA levels (log2)
C Shared STAG1-/STAG2-regulated genes
STAG1
STAG2
RAD21
113
18
115
11
25
25
1178
D Processes and pathways regulated by STAG1/STAG2
STAG1-regulated
STAG2-regulated
GO terms
mitotic cell cycle
nuclear division regulation
circadian pathway
EGFR signaling negative regulation
nervous system development
growth factor cellular response
hypoxia response
E-cadherin stabilization
E2F pathway
Wnt cellular response
chromosome condensation
chondrocyte differentiation
RNA metabolism
wound healing
developmental growth
p63 pathway
wound healing
growth factor cellular response
apoptotic signaling pathway
vascular development
cell junction organization
pinocytosis regulation
response to external stimulus
hypoxia response
E-cadherin stabilization
apoptotic cell clearance
intergin pathway
epidermis development
leukocyte differentiation
stress-activated ERK signaling
-log10(p-value)
-log10(p-value)

Figure S11 STAG1 or STAG2 regulate different genes

A,B) Volcano plots representing the transcriptional changes after STAG1 degradation (A) or STAG2 degradation (B), presented without genes overlapping between the datasets. Significantly changing genes are plotted in green. Genes that lie outside of the plotted range are indicated with their fold change and p-value. **C)** Pie chart showing the overlap of the genes differentially expressed after STAG1, STAG2 and RAD21 degradation (Rao et al. 2017). **D)** Functional analysis of the genes differentially expressed after STAG1 or STAG2 degradation using Metascape (Zhou et al. 2019).

Figure S12

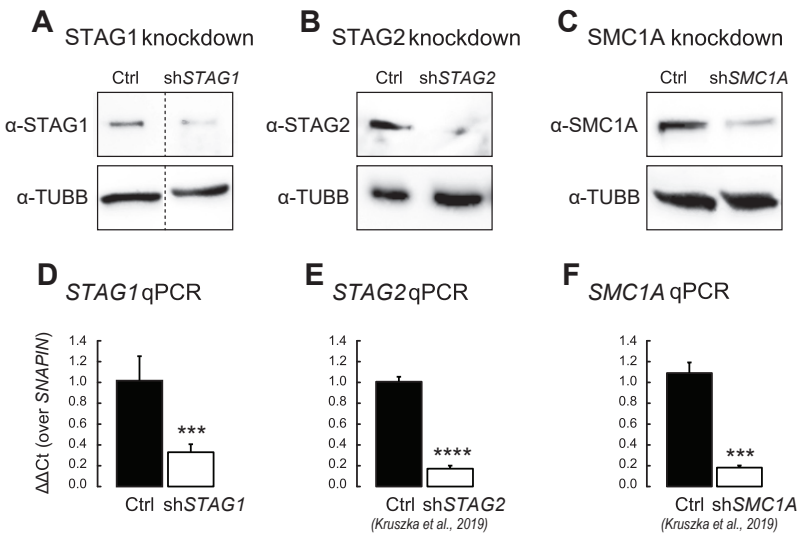
A
STAG1 knockdown
Ctrl
shSTAG1
α-STAG1
α-TUBB
B
STAG2 knockdown
Ctrl
shSTAG2
α-STAG2
α-TUBB
C
SMC1A knockdown
Ctrl
shSMC1A
α-SMC1A
α-TUBB
D
STAG1 qPCR
ΔΔCt (over SNAPIN)
1.4
1.2
1.0
0.8
0.6
0.4
0.2
0.0
***
Ctrl
shSTAG1
E
STAG2 qPCR
1.4
1.2
1.0
0.8
0.6
0.4
0.2
0.0
****
Ctrl
shSTAG2
(Kruszka et al., 2019)
F
SMC1A qPCR
1.4
1.2
1.0
0.8
0.6
0.4
0.2
0.0
***
Ctrl
shSMC1A
(Kruszka et al., 2019)

Figure S12 Depletion of cohesin in neural stem cells

A-**C**) Depletion of STAG1, STAG2 and SMC1A by siRNA-mediated depletion in neural stem cells was confirmed by Western blotting for STAG1 (A), STAG2 (B) and SMC1A (C). Tubulin (TUBB) was used as loading control. **D-F**) Depletion of STAG1, STAG2 and SMC1A by siRNA-mediated depletion in neural stem cells was confirmed by RT-qPCR analysis for the mRNA of *STAG1, STAG2* and *SMC1A. SNAPIN* was used as housekeeping gene. Please note that some of these controls are also shown in Kruska et al. 2019 (Kruszka et al. 2019). (mean of n=3, *t*-test p-values are indicated, *** P< 0.001; **** P < 0.0001).

Figure S13

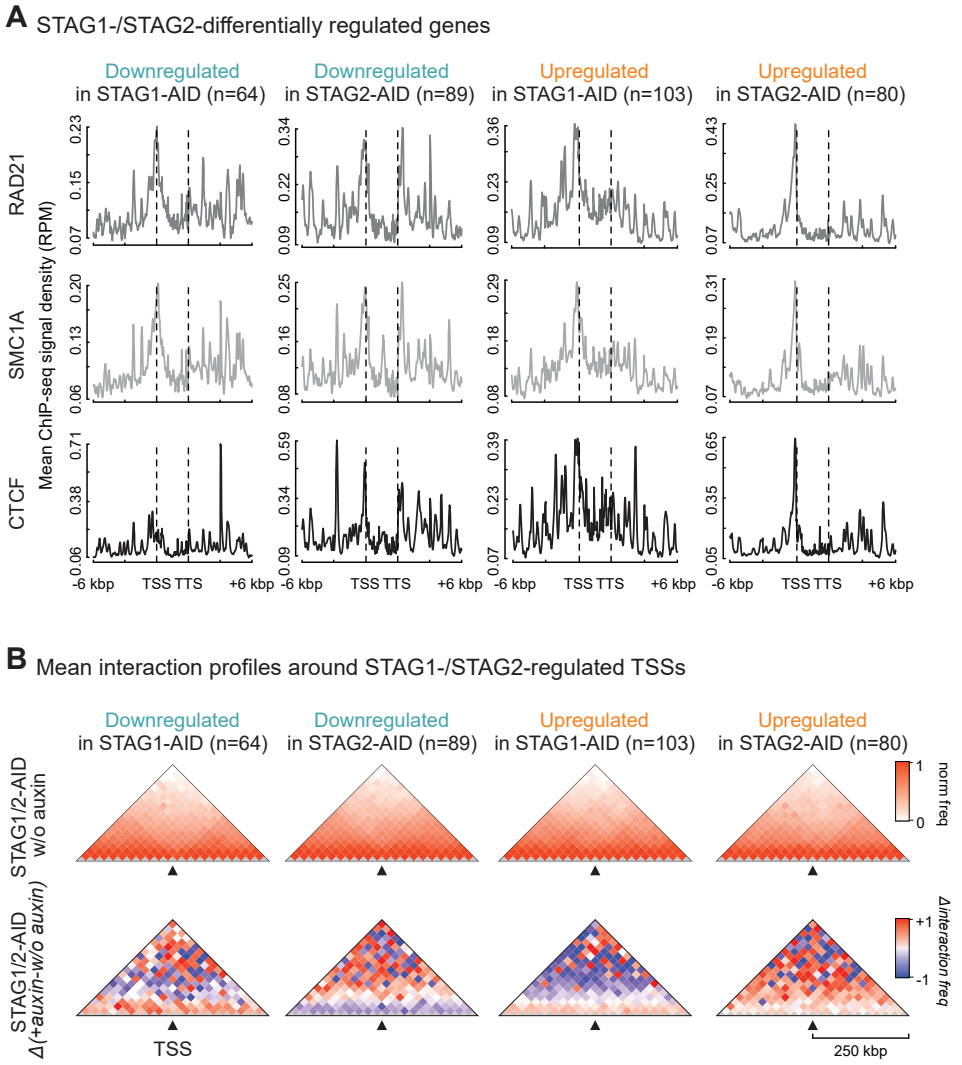
A STAG1-/STAG2-differentially regulated genes
Downregulated in STAG1-AID (n=64)
Downregulated in STAG2-AID (n=89)
Upregulated in STAG1-AID (n=103)
Upregulated in STAG2-AID (n=80)
RAD21
SMC1A
CTCF
Mean ChIP-seq signal density (RPM)
-6 kbp
TSS TTS
+6 kbp
B Mean interaction profiles around STAG1-/STAG2-regulated TSSs
STAG1/2-AID w/o auxin
STAG1/2-AID Δ(+auxin-w/o auxin)
norm freq
Δinteraction freq
TSS
250 kbp

Figure S13 Analysis of gene subsets regulated after auxin-mediated depletion of STAG1 or STAG2

A) Mean RAD21, SMC1A, and CTCF ChIP-seq signal was plotted along the bodies (±6 kbp) of genes specifically up- or down-regulated after depletion of STAG1 or STAG2. **B)** Insulation plots showing mean Hi-C signal from untreated maps (no auxin) around the TSSs of genes specifically up- or down-regulated after depletion of STAG1 or STAG2. For these same TSSs mean changes in Hi-C signal are also plotted. The maps are presented with a bin size of 25 kbp for the 20 bins around each TSS.

Figure S14

A

Loop lenght contacts between SMC3 sites

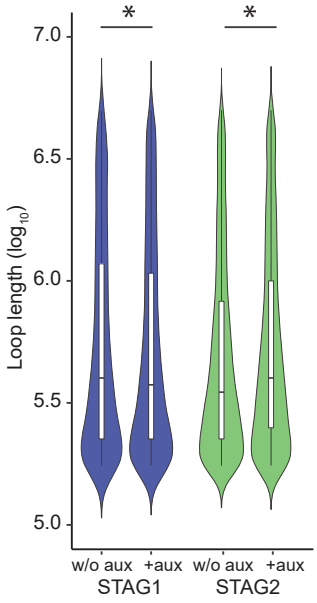

B

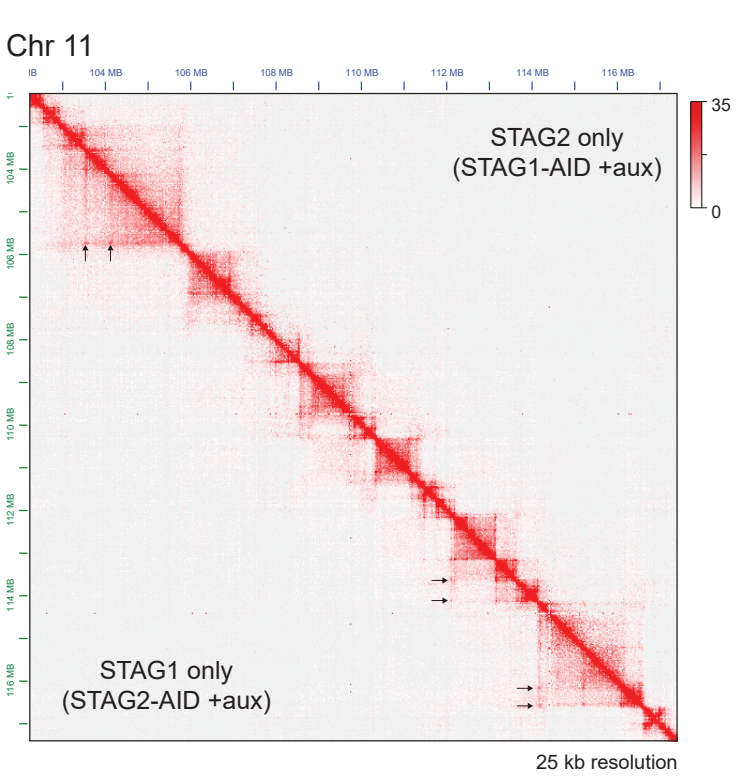

25 kb resolution

C

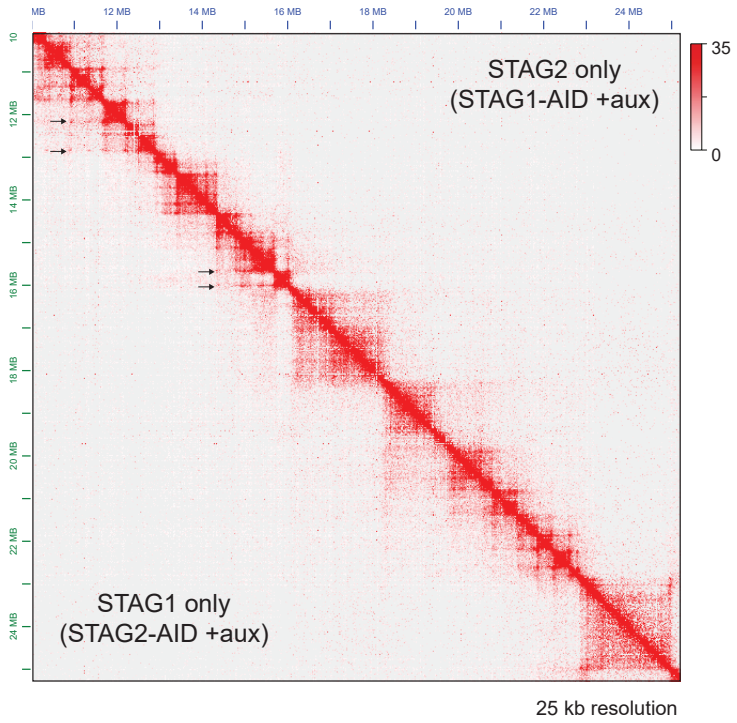

25 kb resolution

Figure S14 STAG1 and STAG2 affects long-range interactions differently

A) Length of the contact loops engaged between SMC3 sites in STAG1-AID and STAG2-AID cells before and after auxin addition. Wilcox test: p value= 0.013 (STAG1) and p value = 0.009 (STAG2). **B-C)** Combined Hi-C maps of cells depending only on STAG1 for their loops (STAG2-AID +auxin) versus Hi-C maps of cells depending only on STAG2 (STAG1-AID +auxin). The maps were generated with Juicebox (Durand et al. 2016) using Balanced (Knight-Ruiz) Hi-C contact frequencies for sections of Chromosomes 11 (B) and 12 (C). Arrows indicate changes.

Figure S15

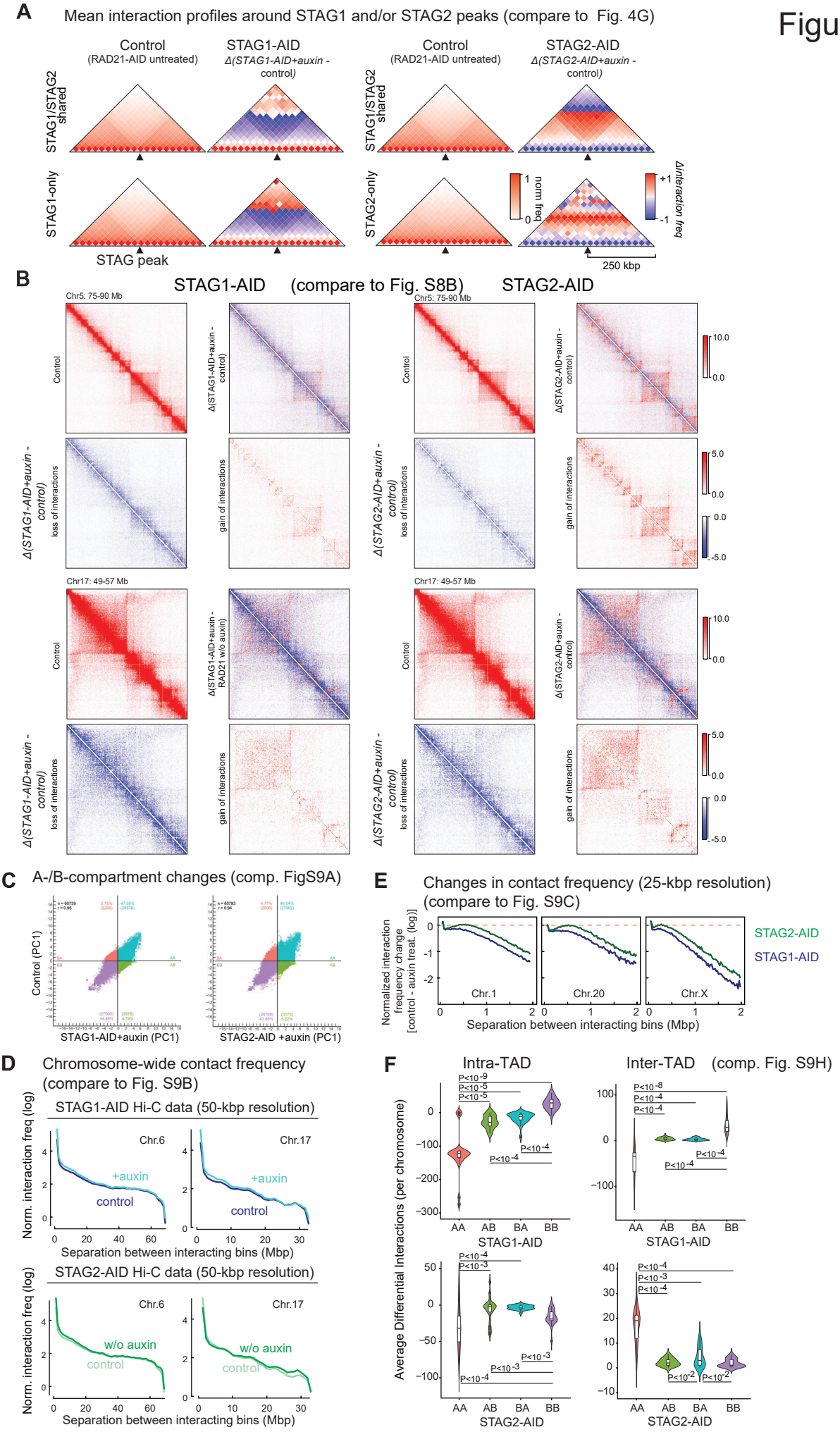
A
Mean interaction profiles around STAG1 and/or STAG2 peaks (compare to Fig. 4G)
Control (RAD21-AID untreated)
STAG1-AID Δ(STAG1-AID+auxin - control)
STAG2-AID Δ(STAG2-AID+auxin - control)
STAG1/STAG2 shared
STAG1-only
STAG2-only
STAG peak
norm freq
Δinteraction freq
250 kbp
B
STAG1-AID (compare to Fig. S8B) STAG2-AID
Chr5: 75-90 Mb
Chr17: 49-57 Mb
Control
Δ(STAG1-AID+auxin - control)
Δ(STAG2-AID+auxin - control)
Δ(STAG1-AID+auxin - RAD21 w/o auxin)
loss of interactions
gain of interactions
C
A-/B-compartment changes (comp. FigS9A)
Control (PC1)
STAG1-AID+auxin (PC1)
STAG2-AID +auxin (PC1)
D
Chromosome-wide contact frequency (compare to Fig. S9B)
STAG1-AID Hi-C data (50-kbp resolution)
STAG2-AID Hi-C data (50-kbp resolution)
Chr.6
Chr.17
+auxin
control
w/o auxin
Norm. interaction freq (log)
Separation between interacting bins (Mbp)
E
Changes in contact frequency (25-kbp resolution) (compare to Fig. S9C)
Normalized interaction frequency change [control - auxin treat. (log)]
Chr.1
Chr.20
Chr.X
STAG2-AID
STAG1-AID
Separation between interacting bins (Mbp)
F
Intra-TAD
Inter-TAD (comp. Fig. S9H)
Average Differential Interactions (per chromosome)
STAG1-AID
STAG2-AID
AA
AB
BA
BB

Figure S15 Use of an alternative "wildtype" control Hi-C dataset for HCT116 cells shows similar chromatin contact changes

Instead of the Hi-C matrices obtained from STAG1-AID and STAG2-AID cells without auxin treatment, we used publicly-available Hi-C data, in the figure referred to as "control" or "control cells" , from untreated RAD21-AID HCT116 (Rao et al., 2017) to assess chromatin organization changes following STAG1 and STAG2 degradation. Despite the caveats of different Hi-C library preparations (6-cutter restriction enzyme in our protocol compared to the 4-cutter used by Rao et al.) and different sequencing depths of the Hi-C libraries (in favour of the Rao et al. data), we still observe the same changes across different scales.

A) Insulation plots showing the averaged Hi-C signals for all STAG1/STAG2 shared peaks as well as all STAG1-only and STAG2-only peaks in the control maps. For the same peaks the averaged differential Hi-C signals in the different maps are shown. The maps are presented with a bin size of 25 kb and 10 bins to the left and right of each binding site.

B) STAG1 and STAG2 affect long-range interactions differently as can be seen in the zoom-in into the contact maps for STAG1-AID cells (left) and STAG2-AID cells (right) for regions on Chromosome 5 and Chromosome 17. The maps for control, auxin-treated STAG1-AID cells and STAG2-AID cells (+auxin) and the differential interaction maps split in loss of interactions (blue) and gain of interactions (red) are shown.

C) Contacts between and within A and B compartments are correlated between the contact matrices of control cells and STAG1-AID and STAG2-AID cells with auxin treatment. Total contacts observed, correlation coefficient as well as the percentage and number of the contacts between the specific compartments are indicated. PC1 = principal component 1.

D) Normalized interaction frequencies are plotted against the distance between interacting bins (at 50 kb resolution) for control and for auxin-treated STAG1-AID and STAG2-AID cells. Chromosomes 6 and 17 are shown.

E) Change of the contact frequencies after STAG1 or STAG2 degradation relative to control cells (at 25 kb resolution) are plotted relative to the separation of the contacting fragments (Chromosomes 1, 20 and X are shown).

F) Intra-TAD or inter-TAD changes of contacts after STAG1 or STAG2 degradation (relative to control cells) between and within A and B compartments. Statistical test performed in E-H: Wilcoxon-Mann-Whitney U test; p-values corrected by the Benjamini-Hochberg method are indicated.

Supplementary references

Davis CA, Hitz BC, Sloan CA, Chan ET, Davidson JM, Gabdank I, Hilton JA, Jain K, Baymuradov UK, Narayanan AK et al. 2018. The Encyclopedia of DNA elements (ENCODE): data portal update. *Nucleic Acids Res* **46**: D794-D801.

Durand NC, Robinson JT, Shamim MS, Machol I, Mesirov JP, Lander ES, Aiden EL. 2016. Juicebox Provides a Visualization System for Hi-C Contact Maps with Unlimited Zoom. *Cell Syst* **3**: 99-101.

Kojic A, Cuadrado A, De Koninck M, Gimenez-Llorente D, Rodriguez-Corsino M, Gomez-Lopez G, Le Dily F, Marti-Renom MA, Losada A. 2018. Distinct roles of cohesin-SA1 and cohesin-SA2 in 3D chromosome organization. *Nat Struct Mol Biol* **25**: 496-504.

Kruszka P, Berger SI, Casa V, Dekker MR, Gaesser J, Weiss K, Martinez AF, Murdock DR, Louie RJ, Prijoles EJ et al. 2019. Cohesin complex-associated holoprosencephaly. *Brain* **142**: 2631-2643.

Lin Q, Chauvistre H, Costa IG, Gusmao EG, Mitzka S, Hanzelmann S, Baying B, Klisch T, Moriggl R, Hennuy B et al. 2015. Epigenetic program and transcription factor circuitry of dendritic cell development. *Nucleic Acids Res* **43**: 9680-9693.

Natsume T, Kiyomitsu T, Saga Y, Kanemaki MT. 2016. Rapid Protein Depletion in Human Cells by Auxin-Inducible Degron Tagging with Short Homology Donors. *Cell Rep* **15**: 210-218.

Natsume T, Muller CA, Katou Y, Retkute R, Gierlinski M, Araki H, Blow JJ, Shirahige K, Nieduszynski CA, Tanaka TU. 2013. Kinetochores coordinate pericentromeric cohesion and early DNA replication by Cdc7-Dbf4 kinase recruitment. *Mol Cell* **50**: 661-674.

Rao SSP, Huang SC, Glenn St Hilaire B, Engreitz JM, Perez EM, Kieffer-Kwon KR, Sanborn AL, Johnstone SE, Bascom GD, Bochkov ID et al. 2017. Cohesin Loss Eliminates All Loop Domains. *Cell* **171**: 305-320 e324.

van der Lelij P, Lieb S, Jude J, Wutz G, Santos CP, Falkenberg K, Schlattl A, Ban J, Schwentner R, Hoffmann T et al. 2017. Synthetic lethality between the cohesin subunits STAG1 and STAG2 in diverse cancer contexts. *Elife* **6**.

Yesbolatova A, Natsume T, Hayashi KI, Kanemaki MT. 2019. Generation of conditional auxin-inducible degron (AID) cells and tight control of degron-fused proteins using the degradation inhibitor auxinole. *Methods* **164-165**: 73-80.

Zhou Y, Zhou B, Pache L, Chang M, Khodabakhshi AH, Tanaseichuk O, Benner C, Chanda SK. 2019. Metascape provides a biologist-oriented resource for the analysis of systems-level datasets. *Nat Commun* **10**: 1523.